Predicting the soil water retention curve from the particle size distribution based on a pore space geometry containing slit-shaped spaces

Chen-chao Chang, Dong-hui Cheng

School of Environmental Sciences and Engineering, Chang'an University, Xi'an, 710054, China;
Key Laboratory of Subsurface Hydrology and Ecological Effects in Arid Region (Chang
'an University), Ministry of Education, Xi' an, China

Correspondence to: Dong-hui Cheng (chdhbsh@chd.edu.cn)

Abstract. Traditional models employed to predict the soil water retention curve (SWRC) from the particle size distribution (PSD) always underestimate the water content in the dry range of the SWRC. Using the measured physical parameters of 48 soil samples from the UNSODA unsaturated soil hydraulic property database, these errors were proven to originate from an inaccurate estimation of the pore size distribution. A method was therefore proposed to improve the estimation of the water content at high suction heads using a pore model comprising a circle-shaped central pore connected to slit-shaped spaces. In this model, the pore volume fraction of the minimum pore diameter range and the corresponding water content were accordingly increased. The predicted SWRCs using the improved method reasonably approximated the measured SWRCs, which were more accurate than those obtained using the traditional method and the scaling approach in the dry range of the SWRC.

1 Introduction

The soil water retention curve (SWRC), which represents the relationship between the water pressure and water content, is fundamental to researching water flow and chemical transport in unsaturated media (Pollacco et al., 2017). Direct measurements of the SWRC consume both time and money (Arya and Paris, 1981; Mohammadi and Vanclooster, 2011), while estimating the SWRC from the particle size distribution (PSD) is both rapid and economical. Therefore, a number of associated conceptual and physical models have been proposed.

The first attempt to directly translate a PSD into an SWRC was performed by Arya and Paris (1981) (here after referred to as the AP model). In this model, the PSD is divided into multiple size fractions and the bulk and particle densities of the natural-structure samples are uniformly applied to each particle size fraction, from which it follows that the pore fraction and the corresponding solid fraction are equal. Thus, the degree of saturation can be set equal to the cumulative PSD function. The soil suction head can be obtained using the capillary equation based on a "bundle of cylindrical tubes" model, and the pore size in the equation is determined by scaling the pore length and pore volume (Arya et al., 2008). Based on the principle

of the AP model, many researchers have focused on improving the suction head calculation, which are commonly based on the capillary equation; but methods that are used to translate the particle diameter into the pore diameter are different (Haverkamp et al., 1986; Zhuang et al., 2001; Mohammadi and Vanclooster, 2011; Jensen et al., 2015). Some models estimate the pore diameter based on the particle packing patterns (e.g., the MV model) (Meskini-Vishkaee et al., 2014),

5   while others utilize the proportionality factor between the pore size and the associated particle diameter (e.g., the HP model and the two-stage approach) (Haverkamp et al., 1986; Jensen et al., 2015). However, the scheme employed to estimate the water content has not been modified and follows the approach of the AP model. The SWRC prediction models which use the same scheme to predict the water content and only improve the suction head calculation are referred to the traditional models in following text.

10   However, these traditional models underestimate the water content in the dry range of the SWRC (Sang and Powers, 2003; Meskini-Vishkaee et al., 2014). Therefore, some researchers have attempted to improve the water content calculation by attributing model errors to both a simplified pore geometry and an incomplete desorption of residual water in the soil pores within a high suction head range (Tuller et al., 1999; Mohammadi and Meskini-Vishkaee, 2012). Recent findings have revealed the existence of corner water, lens water and water films in soils at high matric suction heads (Tuller et al., 1999;

15   Mohammadi and Meskini-Vishkaee, 2012; Or and Tuller, 1999; Shahraeeni and Or, 2010; Tuller and Or, 2005). Therefore, Mohammadi and Meskini-Vishkaee (2012) predicted a SWRC based on the PSD while considering the adsorbed water films and lens water between the soil particles, and slightly improved upon the traditional MV model. Tuller et al. (1999) proposed a pore space geometry containing slit-shaped spaces and derived a corresponding SWRC that considered both the water films and water inside the angular-shaped pores; however, the predicted SWRC failed to describe experimental data at an

20   intermediate water content due to the limitations of the gamma distribution function used to characterize the pore size distribution (PoSD) (Lebeau and Konrad, 2010). Moreover, this model was mathematically complex. Mohammadi and Meskini-Vishkaee (2013) incorporated the residual water content into the MV model and consequently decreased the magnitude of the underestimation in the dry range of the SWRC. However, an accurate estimation of the residual water content remains a challenge. Meskini-Vishkaee et al. (2014) improved the traditional MV model by defining a soil particle

25   packing scaling factor. This method could improve the estimation of the SWRC, and is particularly significant for fine- and medium-textured soils.

Many traditional models are based on a "bundle of cylindrical tubes" representation of the pore space geometry (Arya and Paris, 1981; Zhuang et al., 2001), which results in intrinsic errors when predicting the water flow in variably saturated soils. Consequently, some researchers have considered pore networks as bundles of triangular tubes, which could incorporate

30   the contribution of water in pore corners to the water content (Helland and Skjæveland, 2007). A new pore geometry model comprised of a polygon-shaped central pore connected to slit-shaped spaces was proposed by Tuller et al. (1999) to provide a more realistic representation of natural pore spaces (Tuller et al., 1999; Or and Tuller, 1999; Tuller and Or, 2001). This pore model could represent a foundation for accurately describing the water status in natural soils, particularly in arid environments.

Therefore, the objectives of this study were to evaluate the leading factors that lead to an underestimation of the water content in the dry range of the predicted SWRC using traditional methods and to furthermore propose a method for accurately estimating the water content using a pore space geometry containing slit-shaped spaces to improve the prediction of the SWRC.

5 ## 2 Basic descriptions

The relationship between the PSD and the PoSD is a fundamental element when predicting the SWRC from the PSD. Hwang and Powers (2003) found that the nonlinear relationship between the PSD and the PoSD is more appropriate than the linear relationship applied in the AP model and therefore described both the PSD and the PoSD as lognormal distributions. However, since the PSD and PoSD of soils do not strongly follow a lognormal distribution, this model performed very

10 poorly for moderately fine-textured soils (Hwang and Choi, 2006). Obtaining an accurate PoSD from the PSD of a soil is highly difficult, and the errors that arise from this approach could cause inevitable errors in the predicted SWRC. However, the underestimation of the water content in the dry range of an SWRC has not been comprehensively evaluated from this perspective.

In this study, the measured PoSDs of 48 soil samples were compared with the PoSDs calculated using a traditional

15 model (they were actually the corresponding PSDs) to identify the origins of the errors and their effects on the accuracy of the predicted SWRC. The provided 48 soil samples exhibited a wide range of physical properties (Table 1) and were selected from the UNSODA unsaturated soil hydraulic property database, which contains 790 soil samples with general unsaturated soil hydraulic properties and basic soil properties (e.g., water retention, hydraulic conductivity, soil water diffusivity, PSD, bulk density, and organic matter content) (Nemes et al., 2001). The maximum, minimum and mean values of the soil bulk

20 density and the percentages of clay and sand of the used soil samples for calibration stage were presented in Table 2.

(1) Calculating the PoSD using a traditional model

Traditional models commonly assume that the pore volume fraction of each size fraction can be set equal to the relative solid fraction (Arya and Paris, 1981). Thus, the cumulative pore volume fraction can take the following form:

$$\sum_{j=1}^{j=i} v_j = \sum_{j=1}^{j=i} \omega_j; \qquad i = 1, 2, \cdots\cdots n \tag{1}$$

25 where ω_j is the solid fraction of the jth particle fraction, v_j is the pore volume fraction associated with the jth fraction, and n is the total number of size fractions in the PSD.

The routine procedures employed among the several traditional models to translate a particle diameter into a pore diameter are different. The equivalent pore diameter can be derived from physical properties, including the bulk density and the particle density, or from the proportionate relationship between the pore size and associated particle diameter. Although

30 the former can logically characterize a pore, a complicated pattern can slightly reduce the model performance. While the

latter approach is easy to use, and its rationality has been demonstrated by some researchers (Hamamoto et al., 2011; Sakaki et al., 2014). Here, the latter technique is applied, and it can be expressed as

$$d_i = 0.3D_i \tag{2}$$

where D_i is the mean particle diameter of the ith fraction (μm) and d_i is the corresponding equivalent pore diameter (μm).

5 Inputting the PSD data, then the calculated pore diameters are sequentially paired with corresponding pore volume fractions to obtain a calculated PoSD.

(2) Estimating the PoSD from the SWRC

It is generally difficult to measure the PoSD of a soil; however, the PoSD can be indirectly obtained using the measured water content and suction head (Jayakody et al., 2014). The cumulative pore volume fraction of the ith fraction is equal to

10 the ratio of the measured water content to the saturated water content (Eq. (3)):

$$\theta_i = \theta_s \sum_{j=1}^{j=i} v_j; \qquad i = 1, 2, \cdots \cdots n \tag{3}$$

where θ_s is the saturated water content (cm^3 cm^{-3}) and θ_i is the measured water content (cm^3 cm^{-3}).

Meanwhile, the corresponding pore diameters are derived on the basis of Laplace's equation and Eq. (4):

$$\psi_i = \frac{2\sigma \cos \varepsilon}{r_i g \rho_w} \tag{4}$$

15 where ψ_i is the suction head (mH$_2$O), σ is the surface tension (kg s^{-2}), ε is the contact angle between the soil particle and water, r_i is the pore radius (m), and ρ_w is the density of water (kg m^{-3}). Assuming for water at 20 °C σ=7.275×10^{-2} kg s^{-2}, ρ_w=998.9 kg m^{-3}, g=9.81 m s^{-2}, and ε=0 (Mohammadi and Vanclooster, 2011), then transforming r_i to d_i and substituting numerically the values of the constant yield a simplified expression as Eq. (5):

$$\psi_i = \frac{3000}{d_i} \tag{5}$$

20 where ψ_i is the suction head (cmH$_2$O) and d_i is the pore diameter (μm). Then, the pore diameters calculated by Eq. (5) were sequentially paired with the cumulative pore volume fractions calculated by Eq. (3) to obtain a PoSD, which could be considered a measured PoSD.

The calculated and measured PoSD data were fitted using a modified logistic growth model (Eq. (6)) (Liu et al., 2003):

$$w_i = \frac{1}{1 + a \exp\left(-bd_i^c\right)} \tag{6}$$

25 where w_i is the cumulative pore volume fraction with diameters smaller than d_i (%) and a, b, and c are the fitting parameters (dimensionless). This model produced a good fit for the PoSD data employed in this study with a coefficient of determination (r^2) that ranged from 0.972 to 0.999.

The measured pore volume fraction curves for the typical samples, namely, sand (code: 3172) and clay (code: 2360), and their calculated curves using the traditional model are presented in Fig. 1. The small maps embedded in Fig. 1 exhibit the measured and calculated PoSD curves, which show that the calculated PoSD curves approximately coincide with the measured curves in the larger pore diameter range, while in the smaller range, which corresponds to the higher suction head range on the SWRC, the calculated values are obviously smaller than the measured values. The underestimation of the pore volume fraction in the smaller pore diameter range can consequently lead to an underestimation of the water content at high suction heads. In particular, the calculated pore volume fraction associated with the smallest pore diameter ($d\leq0.6$ μm) was far less than the measured value. These results illustrated that the underestimation of the pore volume fraction with respect to the smallest pore diameter ($d\leq0.6$ μm) was a key factor with regard to the underestimation of the water content in the dry range of the SWRC. In addition, the underestimation of the pore volume fraction is associated with an oversimplified pore space geometry, which traditional models have generally characterized as a bundle of cylindrical capillaries. The measured and calculated pore curves of the other 46 soil samples behaved in the same fashion, and those curves are provided in the Supporting Information (Fig. S1).

3 Improved method

3.1 Estimating the pore volume fraction

In this study, the soil pore structure was conceptualized within a pore model in which the elementary unit cell is composed of a relatively larger circle-shaped central pore connected to two slit-shaped spaces (see Fig. 2). Relative to the polygonal central pore connected to the slit-shaped spaces as described by (Or and Tuller, 1999), both the slit width and the slit length are proportional to the diameter of the associated central pore d and are therefore expressed as αd and βd, respectively.

When estimating the pore volume fraction using the pore model described above, the volume fractions of the central pore and slit-shaped spaces are distinguished. Considering that the sizes of the slit-shaped spaces are smaller than that of the minimum central pore, the slit-shaped spaces are accordingly classified into it. Therefore, the pore volume fractions of the soil samples were simplified into those of the central pores, but the volume fraction of the minimum central pores included that of all slit-shaped spaces. Using the geometric relationship described in Fig. 2 and the traditional assumption that the volume fraction of each unit cell (i.e., the central pore connecting to two slit-shaped spaces) is equal to the corresponding particle mass fraction, the pore volume fractions with respect to different sizes can be readily obtained.

The procedure utilized to calculate the pore volume fractions is shown in Fig. 3. Assuming that the soil pores are composed of numerous unit cells with various sizes, the fraction of the ith unit cell is equal to the relative particle mass fraction ω_i. The addition of the volume fraction of the smallest unit cell (ω_1) and the sum of the slit volume fractions of various sizes ($\zeta_2+\zeta_3+\ldots\ldots+\zeta_i$) results in the volume fraction of the smallest pore (v_1). Successively accumulating it with the volume fractions of other central pore (i.e., v_2, v_3, $v_4\ldots$) provides the PoSD of a sample. The volume fraction of the slit-

shaped spaces, ζ_i, the volume fraction of the smallest pore v_1 and the volume fractions of the other pores v_i were calculated using Eqs. (7), (8) and (9), respectively:

$$\zeta_i = \omega_i \frac{2\alpha\beta d_i^2}{2\alpha\beta d_i^2 + \frac{\pi}{4}d_i^2} \tag{7}$$

$$v_1 = \omega_1 + \sum_{2}^{n} \zeta_i \tag{8}$$

$$v_i = \omega_i - \zeta_i \tag{9}$$

where ζ_i is the volume fraction of the slit-shaped spaces, v_i is the volume fraction of the ith pore fraction, and α and β are the scaling parameters of the slit width and the slit length, respectively.

3.2 Values of α and β

To obtain the values of α and β, an expression containing both of these parameters with respect to the specific surface area (S_{SA}) was applied here. The S_{SA} of the pore as shown in Fig. 2 can be described using a geometrical relationship as follows:

$$S_{SA} = \frac{\phi}{1000\rho_b} \sum_{i=1}^{n} \omega_i \frac{4\beta d_i + \pi d_i}{2\alpha\beta d_i^2 + \frac{\pi}{4}d_i^2}; \qquad i = 1,2,\cdots\cdots n \tag{10}$$

where S_{SA} is the specific surface area (m^2 g^{-1}), d_i is the pore diameter (m), ρ_b is the bulk density (kg m^{-3}) and Φ is the measured porosity. Therefore, an important requirement for the calculation of the α and β values is an estimation of the S_{SA} at sample-scale. Here, a power equation was applied as follows (Sepaskhah et al., 2010):

$$S_{SA} = 3.89 d_g^{-0.905} \tag{11}$$

where S_{SA} is the estimated specific surface area (m^2 g^{-1}), and d_g is the geometric mean particle size diameter (mm) obtained using Eq. (12) (Shirazi and Boersma, 1984):

$$d_g = \exp\left(f_c \ln M_c + f_{si} \ln M_{si} + f_{sa} \ln M_{sa}\right) \tag{12}$$

where f_c, f_{si} and f_{sa} are the clay, silt and sand fractions (%) of the soil sample, respectively, M_c, M_{si} and M_{sa} are the mean diameters of clay, silt and sand that are empirically taken as 0.001 mm, 0.026 mm and 1.025 mm, respectively.

Consequently, the quantitative relationship between the parameters α and β can be obtained using Eq. (10), associated with the additional constraint of Eq. (11), and the values of α and β can be theoretically solved if the measured volume fraction of the slit-shaped pore or the measured SWRC is known. However, an analytical solution is difficult to derive due to the high nonlinearity of both equations. Here, a trial and error approach was adopted that was much easier than the analytical

method. Conveniently, the UNSODA database provided a great deal of soil information, including the measured SWRCs and diverse soil physical properties.

The routine procedure for handling a soil sample involved the following steps. First, given the initial value of α, the value of β was calculated using Eqs. (10)-(12), after which the PoSD was predicted using Eqs. (7)-(9). Subsequently, the SWRC was estimated using the method described in Sect. 3.3. Finally, the values of α were changed repeatedly until the newer predicted SWRC was in good agreement with the measured SWRC and the water content corresponding to a suction head of 5000 cmH$_2$O was within 90% of the measured data (see Fig. S2 in the Supporting Information). The results for the 48 soil samples indicated that the β values exhibited a broad variation range for all samples, while the α values showed regular changes with the soil texture. The relationship between the sand contents and the α values for 48 samples is shown in Fig. 4, which clearly demonstrates that the values of α are similar to samples with specific sand contents.

Therefore, the approach was simplified by setting α as a constant for similar soil textures. The corresponding detailed descriptions are summarized in Table 3. The values of α were inside the range of 3.34E-05 to 2.12E-02, which were estimated by Or and Tuller (1999) using a pore model comprising a polygon-shaped central pore connected to the slit-shaped spaces. According to the sand contents of the samples, Table 3 is a reference for determining the α values that serve as input parameters in predicting the SWRC from the PSD here after.

3.3 Estimating the SWRC

The values of α and β for the various soil samples facilitated the acquisition of the volume fractions of the slit pores using Eq. (7) and the PoSD using Eqs. (8) and (9). The water contents associated with different pore filling stages could be estimated by substituting the PoSD into Eq. (3), and the pore size and the corresponding suction head could be calculated using Eqs. (2) and (5). The SWRC could be ultimately obtained using the calculated suction heads and water contents.

4 Model validation

4.1 Data sources

Twenty-nine soil samples with a wide range of physical properties were also selected from the UNSODA database to validate the model; the codes of the samples are summarized in Table 4 and their detailed information is presented in Table 5. For the soil samples that were not provided with a saturated water content θ_s, the first data point of the measured SWRC corresponding to the lowest suction head was regarded as θ_s.

To generate a detailed PSD, a modified logistic growth model (Eq. (6)) was used to fit the measured PSD data. Here, the detailed PSD was generated at diameter classes of 2, 5, 10, 15, 20, 30, 40, 50, 60, 70, 80, 90, 100, 200, 500, 1000 and 2000 μm. The values of α were chosen from Table 3 according to the sand contents of the soil samples. The values of β were obtained by substituting the S_{SA} values predicted using Eq. (11) into Eq. (10). Then, the PoSD was predicted using Eqs. (7)-(9). Finally, the SWRC was estimated using the methods, as described in Sect. 3.3.

The SWRC was also predicted using the traditional method presented in Sect. 2. In the traditional method, the predicted PoSD was equivalent to the PSD (Eq. (1)) and was substituted into Eq. (3) to obtain the water content. The corresponding suction heads were predicted using Eqs. (2) and (5).

A scaling approach proposed by Meskini-Vishkaee et al. (2014) was used to compare with the proposed method to demonstrate its prediction performance. The detailed calculation procedures were described by Meskini-Vishkaee et al. (2014).

The van Genuchten equation (Eq. (13)) was used to fit the predicted SWRC calculated via the three model (van Genuchten, 1980):

$$\frac{\theta - \theta_r}{\theta_s - \theta_r} = \left[\frac{1}{1 + (a\psi)^n} \right]^m \tag{13}$$

where θ is the water content ($cm^3\,cm^{-3}$), θ_r is the residual water content ($cm^3\,cm^{-3}$), and a, n, m, and θ_r are fitting parameters. The predicted SWRCs of 29 samples exhibited good fits with an average r^2 value of greater than 0.999.

For each set of predictions, the agreement between the predicted and measured water contents was expressed in terms of the root mean square error (E_{RMS}), which is given by

$$E_{RMS} = \sqrt{\frac{1}{N} \sum_{i=1}^{N} (\theta_{pi} - \theta_{mi})^2} \tag{14}$$

where N is the number of measured data points, θ_{pi} is the predicted water content and θ_{mi} is the measured water content.

4.2 Results

The predicted and measured SWRCs in Fig. 5 show that the improved method exhibited good fits with the measured data in the entire range of the SWRC; moreover, the improved method was clearly better than the traditional method and the scaling approach, especially in the dry range (the other 25 samples are listed in Fig. S3 in the Supporting Information). In this study, the scaling approach, which improved the performance of the original MV-VG model via scaling the parameter n in van Genuchten equation, performed better than the traditional method for clay (code:1360), loamy (code: 3190) and loamy sand (code: 3160). However, it performed worse for coarse-textured soil (e. g. sand (code: 3144)), which may result from the relative small scaling degree of the parameter n and the poor fit of the fitting equation to the measured PSD data in their study. In general, the improved method here applied well to a wide range of soils, while the scaling approach performed better for fine- and medium-textured soils.

Table 6 shows the E_{RMS} of the improved method, the scaling approach and the traditional method for samples used in model validation. The E_{RMS} values range from 0.017 to 0.054 for the improved method (with an average of 0.028), from 0.026 to 0.060 for the scaling approach (with an average of 0.037) and from 0.040 to 0.106 for the traditional method (with an average of 0.061). In terms of the E_{RMS}, the improved method provided the best predictions and the traditional method

performed the worst. The results also showed that there is a significant difference between performance of the improved method and traditional method ($p=0.001$). Only for the sand samples does the performance of improved method and scaling approach exhibit a significant statistical difference ($p=0.01$).

The accuracy of the predicted SWRC using the improved method depends on the accuracy of the corresponding
5   predicted pore volume fractions. The calculated and measured pore volume fraction curves in Fig. 6 indicate that the predicted curves using the improved method are more similar to the measured data than those predicted using the traditional method, thereby showing that the proposed method performed better. The errors in the predicted pore fractions using the traditional method mainly occur at the minimum pore size ($d \leq 0.6$ μm), which proves that the errors of the predicted SWRC using the traditional method originate from the neglect of small pores, such as slit-shaped spaces in natural sample. The
10 proposed method used the pore model containing slit-shaped spaces to represent the pore space geometry and consequently improved the prediction of the SWRC. However, the uncertainties are unavoidable when choosing the parameters α for unknown media, which is the main factor affecting the accuracy of the predicted SWRCs.

4.3 Discussion

4.3.1 The suction head calculation in the slit-shaped spaces

15   When capillary water coexists with adsorptive water in the narrow pores, the capillary and surface forces including ionic-electrostatic, molecular, structural, and adsorption forces contribute to the potential energy of water in the slit-shaped pores (Tuller et al., 1999; Iwamatsu and Horii, 1996). When considering only the capillary forces, the drainage potential in slit-shaped pore is given as Eq. (15) (Derjaguin and Churaev, 1992):

$$\mu = \frac{-2\sigma}{\rho \alpha d}$$

(15)

20 where μ is the critical potential (J kg^{-1}).

However, the applicability of this formula is limited by the width of the slit. Tuller and Or (2001) defined a critical slit spacing (αd^*) by Eq. (16) that classifies the slit sizes responding to capillary drainage and adsorption-dominated drainage. In the case of slit-shaped spaces greater than αd^*, the capillary-based slit drainage is applied.

$$\alpha d^* = \sqrt{-\frac{9A_{svl}}{4\pi\sigma}}$$

(16)

25 where A_{svl} is the Hamaker constant for solid-vapor interactions through the intervening liquid, usually set as -6.0E-20 J (Tuller and Or, 2001). The value of αd^* is 0.591 nm, which means that Eq. (15) could be applied to calculate the drainage potential in the slit-shaped spaces in this study.

In our study, the critical drainage suction head for the minimum central pore calculated using Eq.(5) is 5000 cmH$_2$O, while that of the widest slit-shaped spaces calculated using Eq. (15) is 6202 cmH$_2$O (the potential is converted to the suction

head). This result illustrates that all slit-shaped spaces are still filled with water when the suction head is up to the critical drainage suction head for the minimum central pores. On the other hand, the largest slit width calculated from the parameters in Table 3 is 0.24 μm, which is smaller than the minimum pore diameter of 0.6 μm. According to the above analysis, it is reasonable that the volume fractions of the minimum pores include the volume fractions of the minimum central pore and all slit-shaped spaces.

4.3.2 The effects of the estimated S_{SA}

The S_{SA} values estimated using Eq. (11) could affect the accuracy of the predicted SWRCs. Fig. 7 shows that an overestimation of the S_{SA} prompts the dry range of the SWRC to move in the direction of larger water content, and vice versa. When the estimated S_{SA} value was altered by 10% and -10% of its accurate value for loamy sand (code: 3170), the water contents with respect to the highest suction head were higher and lower, respectively, by approximately 0.007 cm^3 cm^{-3} than those of the original SWRC. For clay (code: 4680), the water contents were higher and lower by approximately 0.009 cm^3 cm^{-3} at the same 10% and -10% alterations, respectively. Consequently, for coarse-textured soil, the water content and prediction error of the SWRC changed relatively little for the same degree of change in the S_{SA}. Fig. 7 also showed that a relatively small error appeared between the calculated and measured SWRCs when the error of the estimated S_{SA} was within 20 %.

Previous work has shown that the S_{SA} of soil is closely dependent upon the soil texture and could be estimated from the soil properties and PSD (Sepaskhah and Tafteh, 2013; Resurreccion et al., 2015). The method used to estimate the S_{SA} in Sect. 3.2 was presented by Sepaskhah et al. (2010), who estimated the S_{SA} based on the geometric mean particle size diameter as shown in Eq. (12) with an r^2 value of 0.88. Moreover, the appropriateness of this equation was validated using 64 soil samples by Fooladmand (2011). Sepaskhah et al. (2010) pointed out that the estimation deviations increased distinctly for measured S_{SA} greater than 200 m^2 g^{-1}. In the proposed method, the estimated S_{SA} is mainly used to gain the parameter α and β and to estimate the volume fractions of the slit-shaped spaces; thus, the estimation accuracy of S_{SA} influences the dry range of the SWRC (Fig. 7) and equivalently the degree of improvement in the predicted SWRC. Therefore, more effort should be placed toward developing a more accurate transformation from the soil physical properties to S_{SA} to further improve the prediction of the SWRC.

4.3.3 The slit-shaped spaces and the S_{SA} at the sample scale

Since the central pore diameter d is proportional to the corresponding particle diameter D, the slit width αd, the slit length βd and the specific surface area S_{SAi} of each unit cell are associated with the particle size. The calculated values of αd, βd and S_{SAi} of clay, silt, fine sand and coarse sand particles for the loamy sand (code: 3170) are listed in Fig. 8. The results confirm that the pores formed by bigger soil particles are large with a correspondingly large slit width αd; this is similar to the results of Or and Tuller (1999), and the values are of the same order of magnitude. It is common knowledge that larger soil particles tend to have large surface areas, and therefore, the slit length formed by the contact of soil particle edges should

be relatively long, leading to the positive relationship between the slit length βd and the particle diameter as shown in Fig. 8. This result is different from that in Or and Tuller (1999), where the slit length βd was inversely proportional to the particle diameter. In addition, the S_{SAi} of the ith particle fractions decreased with an increase in the particle diameter, which is consistent with the findings of Or and Tuller (1999) and is in accordance with the general understanding of the S_{SA}.

5 Conclusions

The traditional models employed to translate the PSD into the SWRC underestimate the water content in the dry range of the SWRC. The errors originate from a setting that the cumulative PoSD is equal to the corresponding PSD, which resulted in an underestimate of the pore volume fraction of the minimum pore diameter range and consequently the water content in the dry range of the SWRC. If slit-shaped pore spaces are taken into consideration when estimating the PoSD with a pore model comprising a circle-shaped central pore connected to slit-shaped spaces, the pore volume fraction of the minimum pore diameter range will be accordingly increased; therefore, the SWRC can be more accurately predicted. The estimation of the α and β values is a key step to predicting the SWRC in the proposed method. The α values were obtained using 48 measured soil samples, and those values served as input parameters for predicting the SWRC; then, the β values were readily calculated using a constraint on the estimated S_{SA}. The validation results illustrate that the SWRCs predicted using the proposed method provided the best predictions of the SWRCs, closely followed by the scaling approach, and the traditional method performed worst.

.

Competing interests. The authors declare no conflicts of interest.

Acknowledgments and data

This research was partially supported by the Special Fund for Basic Scientific Research of Central Colleges (310829162015) and by the National Natural Science Foundation of China (41472220). The authors thank Kang Qian for providing the UNSODA unsaturated soil hydraulic property database.

References

Arya, L. M., and Paris, J. F.: A physicoempirical model to predict the soil moisture characteristic from particle-size distribution and bulk density, Soil Science Society of America Journal, 45, 1023-1030, doi:10.2136/sssaj1981.03615995004500060004x, 1981.

Arya, L. M., Bowman, D. C., Thapa, B. B., and Cassel, D. K.: Scaling soil water characteristics of golf course and athletic field sands from particle-size distribution, Soil Science Society of America Journal, 72, 25-32, doi:10.2136/sssaj2006.0232, 2008.

Derjaguin, B. V., and Churaev, N. V.: Polymolecular adsorption and capillary condensation in narrow slit pores, Progress in Surface Science, 40, 173-191, doi: 10.1016/0079-6816(92)90045-J, 1992.

Fooladmand, H. R.: Estimating soil specific surface area using the summation of the number of spherical particles and geometric mean particle-size diameter, African Journal of Agricultural Research, 6(7), 1758-1762, doi: 10.5897/AJAR11.199, 2011.

Hamamoto, S., Moldrup, P., Kawamoto, K., Jonge, L. W. D., Schjønning, P., and Komatsu, T.: Two-region extended archie's law model for soil air permeability and gas diffusivity, Soil Science Society of America Journal, 75(3), 795-806, doi: 10.2136/sssaj2010.0207, 2011.

Haverkamp, R., Parlange, and J., Y.: Predicting the water-retention curve from particle-size distribution: 1. sandy soils without organic matter1, Soil Science, 142, 325-339, doi: 10.1097/00010694-198612000-00001, 1986.

Helland, J. O., and Skjæveland, S. M.: Relationship between capillary pressure, saturation, and interfacial area from a model of mixed-wet triangular tubes, Water Resources Research, 43, 398-408, doi: 10.1029/2006WR005698, 2007.

Hwang, S. I., & Powers, S. E.: Using particle-size distribution models to estimate soil hydraulic properties. Soil Science Society of America Journal, 67(4), 1103-1112, doi:10.2136/sssaj2003.1103, 2003.

Hwang, S. I., and Choi, S. I.: Use of a lognormal distribution model for estimating soil water retention curves from particle-size distribution data, Journal of Hydrology, 323, 325-334, doi: 10.1016/j.jhydrol.2005.09.005, 2006.

Iwamatsu, M., and Horii, K.: Capillary condensation and adhesion of two wetter surfaces, Journal of Colloid & Interface Science, 182, 400-406, doi: 10.1006/jcis.1996.0480,1996.

Jayakody, K. P. K., Shimaoka, T., Komiya, T., and Ehler, P.: Laboratory determination of water retention characteristics and pore size distribution in simulated MSW landfill under settlement, International Journal of Environmental Research, 8, 79-84, doi: 10.22059/IJER.2014.696, 2014.

Jensen, D. K., Tuller, M., Jonge, L. W. D., Arthur, E., and Moldrup, P.: A new Two-Stage Approach to predicting the soil water characteristic from saturation to oven-dryness, Journal of Hydrology, 521, 498-507, doi: 10.1016/j.jhydrol.2014.12.018, 2015.

Lebeau, M., and Konrad, J. M.: A new capillary and thin film flow model for predicting the hydraulic conductivity of unsaturated porous media, Water Resources Research, 46, W12554, doi:10.1029/2010WR009092, 2010.

Liu, J. L., Xu, S. H., and Liu, H.: Investigation of different models to describe soil particle-size distribution data, Advances in Water Science, doi: 10.3321/j.issn:1001-6791.2003.05.010, 2003.

Meskini-Vishkaee, F., Mohammadi, M. H., and Vanclooster, M.: Predicting the soil moisture retention curve, from soil particle size distribution and bulk density data using a packing density scaling factor, Hydrology & Earth System Sciences, 18, 4053-4063, doi: 10.5194/hess-18-4053-2014, 2014.

Mohammadi, M. H., and Vanclooster, M.: Predicting the soil moisture characteristic curve from particle size distribution with a simple conceptual model, Vadose Zone Journal, 10(2), 594-602, doi:10.2136/vzj2010.0080, 2011.

Mohammadi, M. H., and Meskini-Vishkaee, F.: Predicting the film and lens water volume between soil particles using particle size distribution data, Journal of Hydrology, 475, 403-414, doi:10.1016/j.jhydrol.2012.10.024, 2012.

Mohammadi, M. H., and Meskini-Vishkaee, F.: Predicting soil moisture characteristic curves from continuous particle-size distribution data, Pedosphere, 23, 70-80, doi: 10.1016/S1002-0160(12)60081-2, 2013.

Nemes, A., Schaap, M. G., Leij, F. J., and Wösten, J. H. M.: Description of the unsaturated soil hydraulic database UNSODA version 2.0, Journal of Hydrology, 251, 151-162, doi: 10.1016/S0022-1694(01)00465-6, 2001.

Or, D., and Tuller, M.: Liquid retention and interfacial area in variably saturated porous media: Upscaling from single-pore to sample-scale model, Water Resources Research, 35, 3591-3605, doi: 10.1029/1999WR900262, 1999.

Pollacco, J. A. P., Webb, T., Mcneill, S., Hu, W., Carrick, S., Hewitt, A., and Lilburne, L.: Saturated hydraulic conductivity model computed from bimodal water retention curves for a range of New Zealand soils, Hydrology & Earth System Sciences, 21, 1-27, doi: org/10.5194/hess-21-2725-2017, 2017.

Resurreccion, A. C., Moldrup, P., Tuller, M., Ferré, T. P. A., Kawamoto, K., Komatsu, T., and Jonge, L. W. D.: Relationship between specific surface area and the dry end of the water retention curve for soils with varying clay and organic carbon contents, Water Resources Research, 47, 240-250, doi: 10.1029/2010WR010229, 2015.

Sakaki, T., Komatsu, M., and Takahashi, M.: Rules-of-Thumb for predicting air-entry value of disturbed sands from particle size, Soil Science Society of America Journal, 78, 454, doi:10.2136/sssaj2013.06.0237n, 2014.

Sepaskhah, A. R., Tabarzad, A., and Fooladmand, H. R.: Physical and empirical models for estimation of specific surface area of soils, Archives of Agronomy & Soil Science, 56, 325-335, doi: 10.1080/03650340903099676, 2010.

Sepaskhah, A. R., and Tafteh, A.: Pedotransfer function for estimation of soil-specific surface area using soil fractal dimension of improved particle-size distribution, Archives of Agronomy and Soil Science, 59, 1-11, doi: 10.1080/03650340.2011.602632, 2013.

Shahraeeni, E., and Or, D.: Pore-scale analysis of evaporation and condensation dynamics in porous media, Langmuir the Acs Journal of Surfaces & Colloids, 26, 13924-13936, doi: 10.1021/la101596y, 2010.

Shirazi, M. A., and Boersma, L.: A unifying quantitative analysis of soil texture, Soil Science Society of America Journal, 48, 142-147, doi: 10.2136/sssaj1984.03615995004800010026x, 1984.

Tuller, M., Or, D., and Dudley, L. M.: Adsorption and capillary condensation in porous media: Liquid retention and interfacial configurations in angular pores, Water Resources Research, 35, 1949–1964, doi: 10.1029/1999WR900098, 1999.

Tuller, M., and Or, D.: Hydraulic conductivity of variably saturated porous media: Film and corner flow in angular pore space, Water Resources Research, 37, 1257-1276, doi: 10.1029/2000WR900328, 2001.

Tuller, M., and Or, D.: Water films and scaling of soil characteristic curves at low water contents, Water Resources Research, 41, 319-335, doi: 10.1029/2005WR004142, 2005.

van Genuchten, M. T.: A closed-form equation for predicting the hydraulic conductivity of unsaturated soils, Soil Science Society of America Journal, 44, 892-898, doi:10.2136/sssaj1980.03615995004400050002x, 1980.

5   Zhuang, J., Jin, Y., and Miyazaki, T.: Estimating water retention characteristic from soil particle-size distribution using a non-similar media concept, Soil Science, 166, 308-321, doi: 0038-075C/01/16605-308–321, 2001.
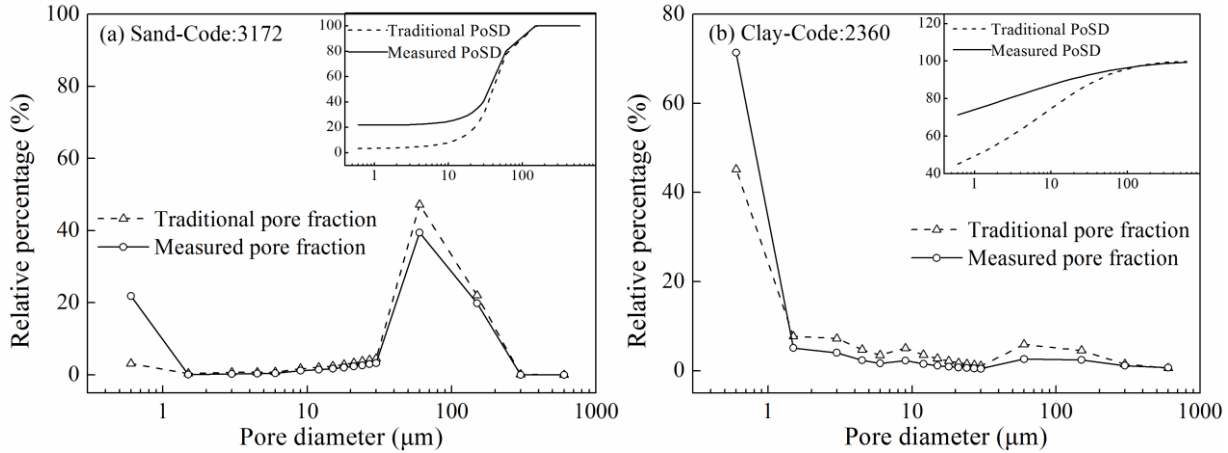
Figure 1: Measured vs. calculated pore volume fraction curves for (a) sand (code: 3172) and (b) clay (code: 2360). The measured
15   **and calculated PoSDs are in the insets at the top of the figures.**
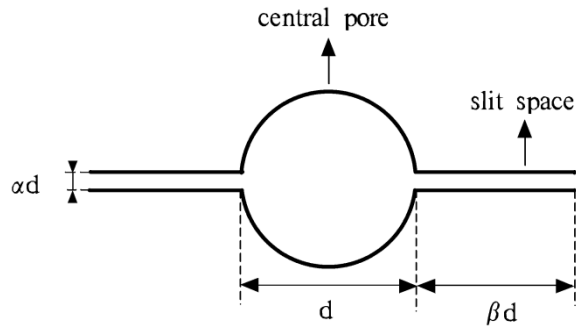
Figure 2: Pore model containing two slit-shaped spaces (*d* denotes the diameter of the central pore, and *αd* and *βd* denote the

widths and lengths of the slit-shaped spaces, respectively).
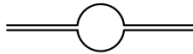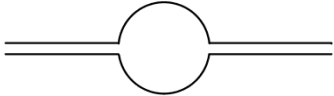
	Formed pores	PSD	Volume fraction of slit–shaped spaces	Volume fraction of pores
$d_1 \leqslant 0.6\,\mu m$		ω_1		$v_1 = \omega_1 + \zeta_2 + \cdots + \zeta_i$
d_2		ω_2	ζ_2	$v_2 = \omega_2 - \zeta_2$
$\vdots$	$\vdots$	$\vdots$	$\vdots$	$\vdots$
d_i		ω_i	ζ_i	$v_i = \omega_i - \zeta_i$

Figure 3: Schematic of the procedure used to calculate the pore volume fraction.
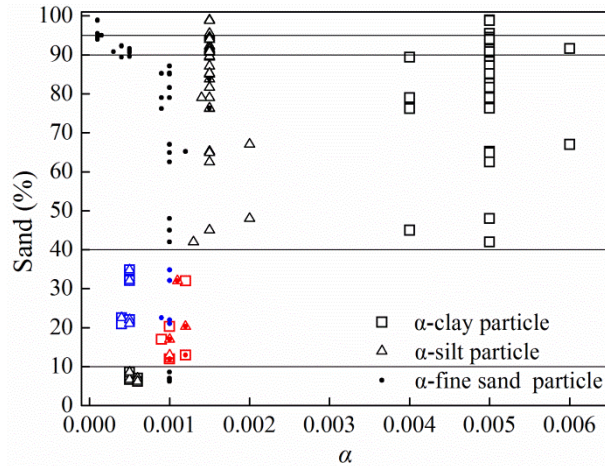
Figure 4: The α values for 48 soil samples with different sand content. The α values for clay, silt, and fine sand particle of specific samples are listed in Fig. 4 except those of the coarse sand particle, which are the same value of 0.0004 for all of the samples. For the samples with sand content ranging from 10-40%, two sets of α value are observed. The α values for the silt content less than and more than 50% are highlighted in red and blue, respectively, thereby reflecting the dominant functions of the silt or clay particle on the hydraulic properties of typical samples.
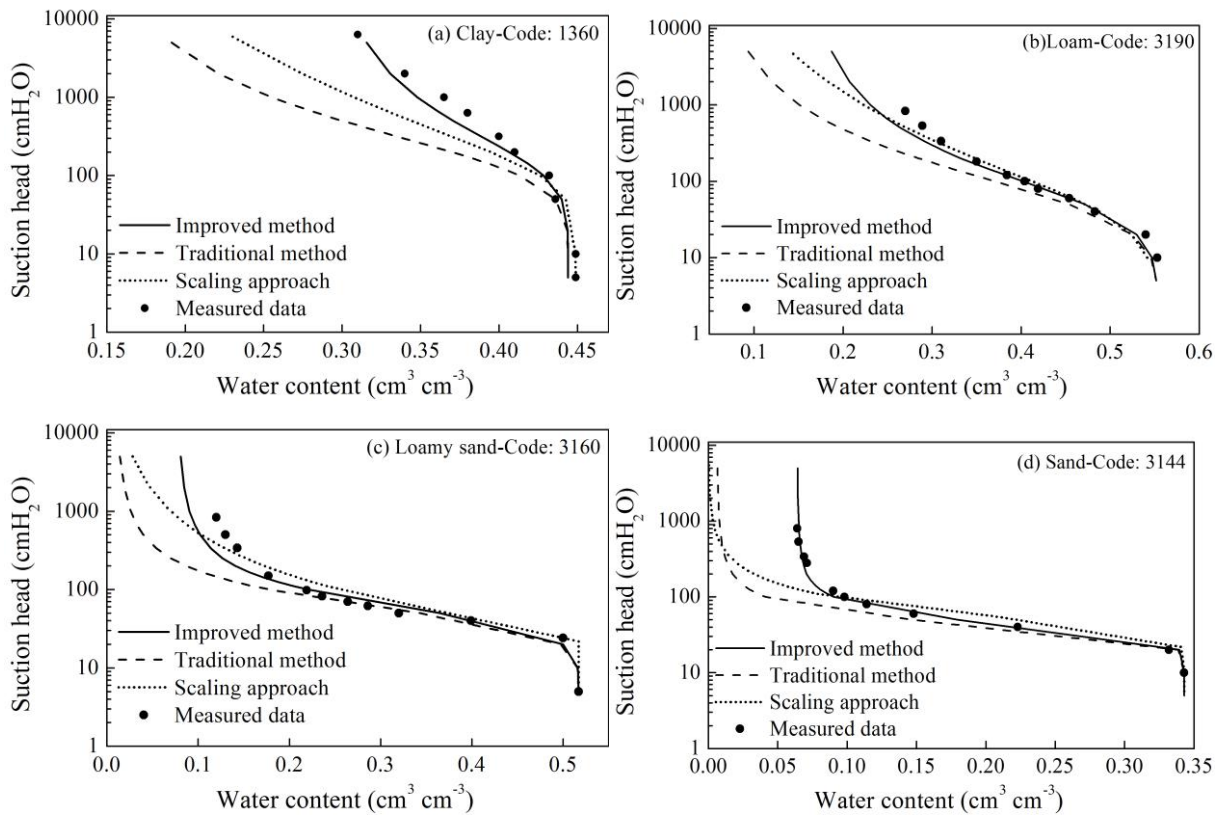
Figure 5: Measured and predicted SWRCs for clay (code: 1360), loam (code: 3190), loamy sand (code: 3160) and sand (code: 3144).
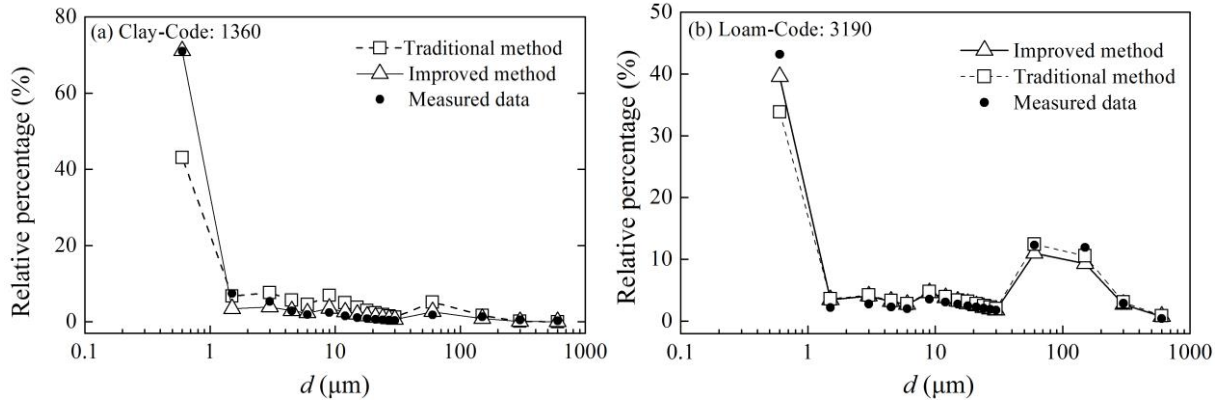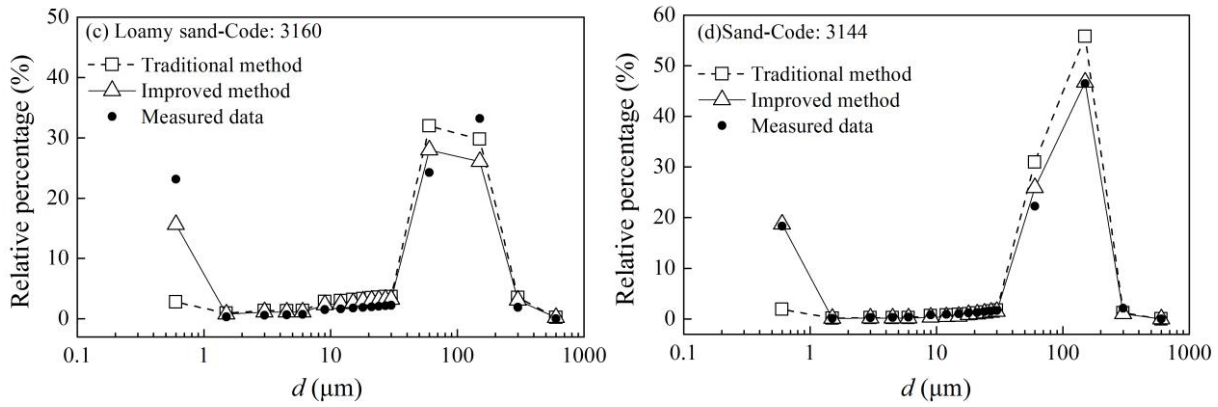
Figure 6: The measured and predicted pore volume fraction curves using the improved method and traditional method for clay (code: 1360), loam (code: 3190), loamy sand (code: 3160) and sand (code: 3144).
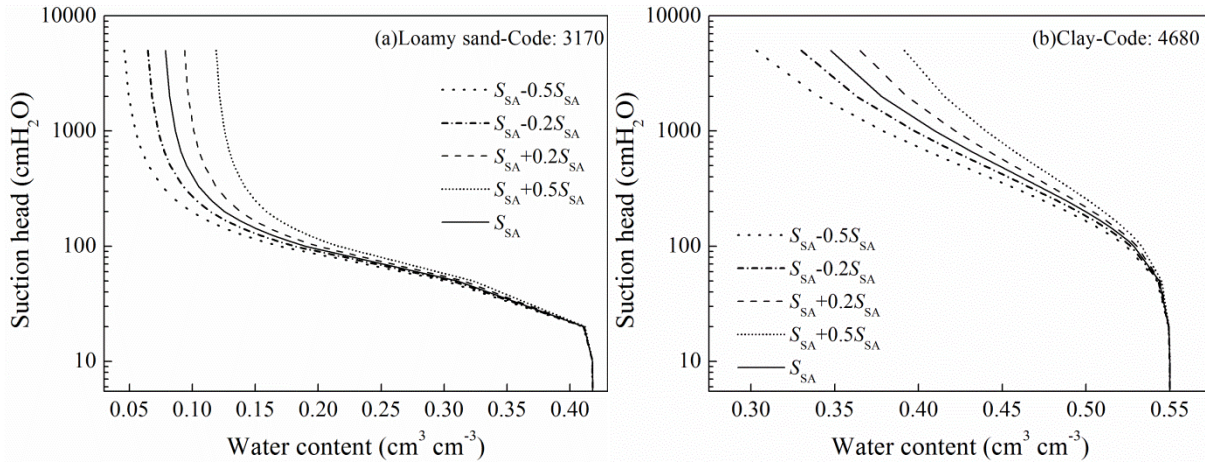
Figure 7: The effects of a change in the estimated S_{SA} on the SWRC for loamy sand (code: 3170) and clay (code: 4680). The S_{SA} denotes the accurate value of the specific surface area.

Loamy sand−Code: 3170		$S_{SA}=8.19$ m^{2}g^{-1}		
Particle size fraction	Formed pores	α d (m)	β d (m)	S_{SAi} (m^{2}g^{-1})
Clay	d⩽0.6 μm	3E−9	0.00004	4.98
Silt	0.6 μm< d ⩽15μm	1.4E−8	0.00056	1.91
Fine sand	15 μm< d ⩽150 μm	8.4E−8	0.0051	1.29
Coarse sand	150 μm< d ⩽600 μm	1.2E−7	0.0178	0.006

Figure 8: The calculated slit width αd, slit length βd and S$_{SAi}$ for loamy sand (code: 3170).

Table 1: Codes and texture classes of the 48 soils selected from UNSODA

UNSODA codes	Texture class
4681, 4680, 2362, 2360, 1400, 1383, 4121, 1361, 2340	Clay
3191, 1091, 2530, 2531	Loam
2102, 3150, 3161, 3171, 1160, 3170, 3130, 1031, 4011, 4020	Loamy sand
1464, 1466, 2100, 3340, 4650, 3142, 1050, 1023, 3141, 3163, 3164, 3165, 3172, 4051, 4520, 4521	Sand
3202	Sandy clay loam
3200, 3203, 4162	Sandy loam
4042, 4180, 4070, 4673, 1341	Silt loam

Table 2: Basic soil properties of 48 samples for the model calibration

Soil texture	Number of soil samples		Clay (%)	Sand (%)	ρ_b (g cm^{-3})
Clay	9	Min	41.5	6.1	1.08
		Max	58.2	36.0	1.64
		Average	50.2	14.1	1.29
Loam	4	Min	14.0	42.0	1.36
		Max	23.0	67.0	1.63
		Average	17.3	50.5	1.46

Loamy sand	10	Min	3.0	76.2	1.32
		Max	10.4	89.4	1.60
		Average	6.1	83.2	1.46
Sand	16	Min	0.7	89.6	1.41
		Max	4.6	98.9	1.70
		Average	2.5	93.4	1.55
Sandy clay loam	1		2.7	62.5	1.70
Sandy loam	3	Min	10.5	64.9	1.27
		Max	19.4	76.3	1.70
		Average	15.0	68.8	1.50
Silt loam	5	Min	10.5	21.0	1.49
		Max	15.7	34.8	1.56
		Average	12.6	26.5	1.52

Table 3: The estimated values of α for various soil textures

Sand content (%)	Silt content (%)	α			
		Clay $D\leq2$ μm	Silt 2 μm$<D\leq50$ μm	Fine sand 50 μm$<D\leq500$ μm	Coarse sand 500 μm$<D\leq2000$ μm
0-10		0.0005	0.0005	0.001	0.0004
10-40	0-50	0.001	0.001	0.001	0.0004
	50-100	0.0005	0.0005	0.001	0.0004
40-90		0.005	0.0015	0.001	0.0004
90-95		0.005	0.0015	0.0005	0.0004
95-100		0.005	0.0015	0.0001	0.0004

Table 4: Codes of the 29 soil samples selected from UNSODA for the model validation

UNSODA codes	Texture class
1360, 4120, 2361, 3282, 1320	Clay
3190, 1370	Loam
3160, 3152, 1030, 1090, 4010	Loamy sand
3155, 3144, 1463, 3132, 4000	Sand
4620, 4621, 1102, 2341	Sandy clay loam
3290, 3310	Sandy loam
4531, 4510	Silt loam
3031, 3032, 1372, 1362	Clay loam

Table 5: Basic soil properties of 29 samples for the model validation

Soil texture	Number of soil samples		Clay (%)	Sand (%)	ρ_b (g cm^{-3})
Clay	5	Min	43.0	5.4	1.10
		Max	57.0	32.0	1.50
		Average	51.0	14.4	1.31

Loamy	2	Min	16.5	47.9	1.41
		Max	29.2	43.6	1.45
Loamy sand		Min	1.7	75.5	1.37
	5	Max	7.3	85.2	1.59
		Average	4.9	81.0	1.46
Sand		Min	1.1	90.1	1.46
	5	Max	4.4	97.5	1.58
		Average	2.3	93.4	1.53
Sandy loam	2	Min	11.4	56.8	1.44
		Max	12.6	65.7	1.46
		Min	9.8	28.0	1.21
Sandy clay loam	6	Max	30.7	69.7	1.53
		Average	22.8	43.2	1.45
		Min	33.4	20.4	1.07
Clay loam	4	Max	37.5	34.7	1.58
		Average	35.1	24.8	1.27

Table 6: The root mean square errors (E_{RMS}) of the predicted SWRC using the improved method, the scaling approach and the traditional method

Soil texture	Number of soil samples	E_{RMS}		
		Improved method	Scaling approach	Traditional method
Clay	5	0.022	0.032	0.056
Clay loam	4	0.034	0.041	0.079
Sandy clay loam	4	0.032	0.046	0.072
Loam	2	0.054	0.060	0.106
Loamy sand	5	0.020	0.026	0.048
Sand	5	0.017	0.028	0.042
Sandy loam	2	0.046	0.049	0.068
Silt loam	2	0.024	0.031	0.040